Pattern formation in a two-dimensional reaction-diffusion channel with Poiseuille flow

Pavel V. Kuptsov*

Department of Informatics, Saratov State Law Academy, Chernyshevskaya 104, Saratov 410056, Russia

Razvan A. Satnoianu

Faculty of Actuarial Science, Cass Business School, City University, London EC1Y 8TZ, United Kingdom

Peter G. Daniels

Centre for Mathematical Science, City University, Northampton Square, London EC1V 0HB, United Kingdom

We study stationary patterns arising from a combination of flow and diffusion in a two-dimensional (2D) reaction-diffusion system in a channel with Poiseuille flow. Both transverse and longitudinal modes are investigated and compared with numerical computations.

I. INTRODUCTION

Flow- and diffusion-distributed structures (FDS) are stationary periodic patterns that appear in reaction-diffusion systems with open flow if a constant perturbation from a uniform steady state is applied at the inlet [1,2]. Unlike Turing patterns [3] and differential-flow instability (DIFI) [4], such structures can be observed even for identical diffusion and flow rates of the reactants. The mechanism of formation of these structures was discovered theoretically by Kuznetsov *et al.* [1] and subsequently Andresén *et al.* [2] identified its important role as a new model of pattern formation. Soon after the theoretical discovery these structures were first obtained in an experiment by Kærn and Menzinger [5]. They studied a system without differential transport and, to underline the kinematic nature of the observed patterns, referred to them as flow-distributed oscillations (FDO). The role of differential transport was later studied by Satnoianu *et al.* [6,7] and by McGraw and Menzinger [8]. Generalized structures of this kind became known as FDS, and Míguez *et al.* [9] carried out the first experimental observation of such structures. Now FDS patterns attract much interest. Theoretical [10–13] and experimental [14–17] studies have addressed different properties of these structures. Also, the FDS mechanism is relevant in biological systems [18,19].

All previous theoretical studies of FDS were made for a 1D model system. Experiments were also carried out for systems with negligible transverse variations in flow rate and chemical concentrations [5,14,15]. This situation is rather artificial and in our paper we introduce a more realistic 2D model that employs a channel with a parabolic velocity profile (Poiseuille flow [20]).

The only experiment with a Poiseuille flow was published by Kærn and Menzinger [5]. The experiment was unsuccessful and Kærn and Menzinger concluded that flow-distributed oscillations cannot be obtained in a system with a parabolic velocity profile. However, we believe that this problem should be studied in more detail and in the present paper the possible existence of such structures is examined numerically and analytically.

II. FORMULATION

We consider as a model system the 2D version of the well-known Lengyel-Epstein equations for the CIMA (chlorite-iodide-malonic acid-starch) reaction [7,21,22]:

$$u_t + \Phi(y)u_x - \Delta u = a - u - 4uv/(1 + u^2), \quad (1a)$$

$$v_t + \Phi(y)v_x - \delta\Delta v = b[u - uv/(1 + u^2)]. \quad (1b)$$

Here $u \equiv u(x,y,t)$ and $v \equiv v(x,y,t)$ are the dimensionless dynamical variables related to the interacting chemical species, $a > 0$ and $b > 0$ are constant parameters related to the chemical species, Δ is the 2D Laplacian, and $\delta > 0$ is the ratio of the diffusion rates for v and u. Subscripts denote partial derivatives and $\Phi(y)$ is the velocity profile of the flow along the channel in the x direction. For Poiseuille flow,

$$\Phi(y) = \phi(1 - y^2/h^2), \quad -h \leq y \leq h, \quad (2)$$

where $\phi > 0$ is the central flow rate and $2h$ is the width of the channel. The geometry of our model is shown in Fig. 1. At the walls of the channel it is assumed that the flux of chemical species vanishes:

$$u_y(x,y = \pm h,t) = v_y(x,y = \pm h,t) = 0. \quad (3)$$

The system (1)–(3) admits the homogeneous steady-state solution $u_S = a/5$, $v_S = 1 + a^2/5^2$. In the absence of flow ($\Phi = 0$) this is destabilized by the Hopf or Turing modes whose growth rates become positive at the critical points,

$$b_H = (3a^2 - 125)/(5a) \quad (4)$$

and

$$b_T = \delta[125 + 13a^2 - 4a\sqrt{10(25 + a^2)}]/(5a), \quad (5)$$

*Corresponding author. Electronic address: kupav@mail.ru
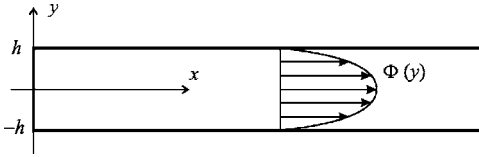
FIG. 1. Sketch of a 2D reactor with parabolic Poiseuille flow.

respectively [3,21,22]. Hopf instability results in uniform temporal oscillations while Turing instability produces a stationary pattern. The Turing instability can be observed only if the differential diffusion coefficient δ is sufficiently high [3]. Note that instability occurs for values of b below the critical points (4) and (5).

In the 1D case, where (2) is replaced by $\Phi = \phi$ with ϕ constant, FDS solutions are obtained by applying a constant perturbation at the inlet. The transition to FDS takes place if the flow rate is above a critical value. The results of a linear stability analysis show that the critical flow rate and corresponding wave number are [1,2,12]

$$\phi_{FDS} = \sqrt{\frac{40a^3b(\delta+1)^2 - (3a^2\delta + 5ab - 125\delta)^2}{(25+a^2)(\delta+1)(3a^2 - 5ab - 125)}}, \quad (6)$$

$$k_{FDS} = \sqrt{\frac{(3a^2 - 5ab - 125)}{(25+a^2)(\delta+1)}}. \quad (7)$$

Note that ϕ_{FDS} diverges and k_{FDS} vanishes at $b = b_H$, i.e., in the 1D case the FDS domain coincides with the Hopf domain [6].

III. NUMERICAL RESULTS

In this section we report the numerical solutions of (1)–(3). The solutions are obtained using the Peaceman-Rachford method of variable directions [23]. To produce pattern formation in our 2D flow system, we apply constant boundary conditions at the inlet,

$$u(x=0,y,t) = u_S + U_{bnd}(y), \quad (8a)$$

$$v(x=0,y,t) = v_S + V_{bnd}(y), \quad (8b)$$

where at least one of the profiles $U_{bnd}(y)$ and $V_{bnd}(y)$ is nonzero. In most of the numerical experiments reported here a uniform inlet perturbation is taken and, in general, it is assumed that $U'_{bnd}(y=\pm h) = V'_{bnd}(y=\pm h) = 0$, consistent with (3). Also, an outlet condition $(u_{xx},v_{xx})_{x=X} = 0$ is applied, where X is the length of the reactor.

Typically, in numerical experiments with our 2D model stationary patterns of two types are encountered: stripes transverse to the flow and longitudinal stripes. Transverse solutions correspond to y-dependent versions of FDS in 1D systems, while longitudinal ones are specific to the 2D case.

Figure 2 shows some typical transverse patterns obtained when the flow rate is sufficiently high. In Fig. 2(a) the width of the reactor is small ($h=1.5$) and the pattern is similar to that of a 1D FDS structure. The transverse stripes are uniform, i.e., have almost constant width and only slight curva-
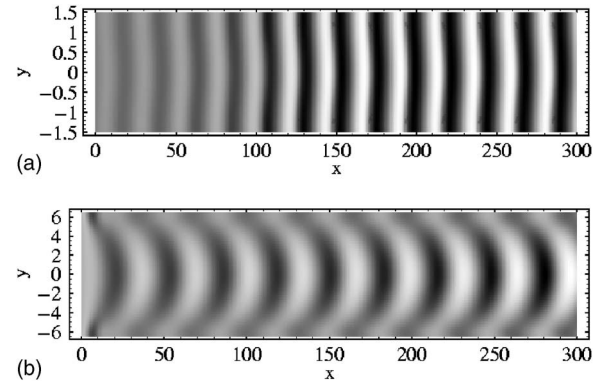
FIG. 2. Transverse steady-state solutions to the system (1)–(3) at $a=30$, $b=12$, $\delta=3$, and $\phi=17$. Gray levels are proportional to the values of u: the lighter tone represents higher values. (a) $h=1.5$, (b) $h=6.5$. $U_{bnd}(y) \equiv 0.5$, $V_{bnd}(y) \equiv 0$.

ture associated with the y dependence of the flow. However, an increase in the value of h results in some significant changes. Figure 2(b) shows the transverse pattern for $h=6.5$. The stripes are now nonuniform. In the middle they are thick with more or less constant width and small curvature whereas the ends are thin and more curved. This suggests the development of a boundary-layer structure as $h \to \infty$.

The mechanism of transverse pattern formation is similar to that of the 1D case. These patterns appear in the Hopf instability domain. Flow and diffusion are responsible for the distribution of the Hopf oscillation in space while the constant condition at the inlet fixes the initial phase and provides the stationarity of the pattern. In addition, transverse diffusion synchronizes the solution across the channel so that the pattern extends into the regions of slow flow near the walls.

Our simulations show that, similar to the 1D case, the transverse solution appears when the flow rate is above a critical value ϕ_t and that the corresponding critical wave number k_t is nonzero. The behavior of ϕ_t and k_t as functions of h is quite interesting and is analyzed in Sec. IV.

Figure 3 illustrates a longitudinal solution. Figure 3(a) shows how the stationary pattern forms behind a moving
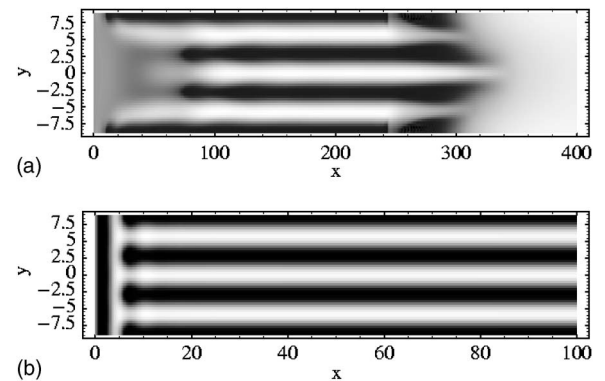
FIG. 3. Longitudinal solutions for $n=6$. $a=30$, $b=12$, $\delta=9$, $h=9$, $U_{bnd}(y) \equiv 0.5$, $V_{bnd}(y) \equiv 0$. (a) is a snapshot of the formation of the stationary pattern behind the moving arrowed front, $\phi=25$. (b) is the steady state for $\phi=0$ when the structure (a) is taken as the initial state.

(a)

(b)
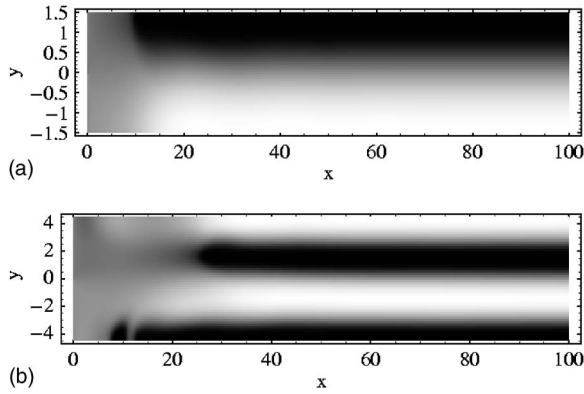
FIG. 4. Odd longitudinal solutions forced by the inlet profiles $U_{bnd}(y)=0.5$ sign(y) and $V_{bnd}(y) \equiv 0$. $a=30$, $b=12$, $\delta=9$, $\phi=10$. (a) $h=1.5$, $n=1$, (b) $h=4.5$, $n=3$.

front that has an arrowlike structure. Unlike the transverse stripes, the flow is not vitally important for the longitudinal solution. Figure 3(b) indicates that this solution survives, even when $\phi=0$. Though an arbitrary initial state results in a traveling wave solution, a fully developed longitudinal pattern obtained for $\phi>0$ remains nearly unaltered if the flow vanishes. The modifications mostly concern the boundary layer near the inlet, which becomes much shorter when the flow rate is reduced.

The longitudinal solutions, unlike the transverse ones, are specific to the 2D case. As we analyze in Sec. IV, the longitudinal pattern is associated with the Turing instability because, from (1), the flow $\Phi(y)$ has no effect on a solution for u and v that is independent of x. Transport in the longitudinal direction synchronizes the solution in that direction and produces a structure homogeneous in x.

The number of stripes in the longitudinal solution depends on h. It is convenient to count these solutions with index n. This index gives the number of inflections of u and v in the y direction so that $n+1$ is the number of lighter and darker stripes. An even index corresponds to an axially symmetric profile $u(-y)=u(y)$, while an odd index corresponds to a profile with odd symmetry $u(-y)=-u(y)$. For the solutions in Fig. 3, $n=6$.

The longitudinal solutions with n odd are difficult to obtain when the inlet profiles are uniform in y because they force the axially symmetric modes of the system. Odd inlet profiles, however, can produce odd solutions, as shown in Fig. 4, where use of the step function at the inlet results in the growth of odd solutions with $n=1$ and $n=3$. Higher odd values of n require the use of more complicated inlet profiles because these solutions are more easily damped by the even modes.

When the transverse and longitudinal modes appear simultaneously, the interaction between them results in the formation of more complicated patterns. Figure 5 presents an example of this. In Fig. 5(a) the flow rate is far below the critical point for the transverse solution ϕ_t, and the space is occupied by the longitudinal stripe that exists at any ϕ. The toothlike pattern along the edges of the stripe is nonstationary and travels in the x direction. In Fig. 5(b) the transverse solution appears, since ϕ exceeds the critical value ϕ_t. The

(a)

(b)
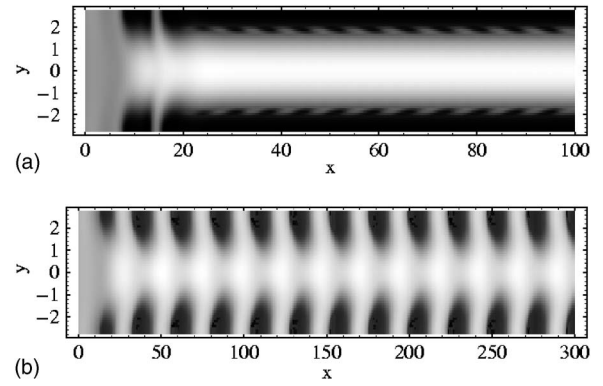
FIG. 5. Transition from the longitudinal solution (a) to the transverse one when the flow rate grows. $a=30$, $b=12$, $\delta=9$, $h=2.8$, $U_{bnd}(y) \equiv 0.5$, $V_{bnd}(y) \equiv 0$. (a) $\phi=5$, (b) $\phi=18$ ($\phi_t \approx 16.0$). The solution in (b) is stationary, while in (a) the toothlike pattern travels in the x direction.

longitudinal solution is still admitted and, being partially damped, is manifested as a raised area along the axis of the reactor.

Figure 6 shows another example of the interaction between the modes: a remarkable spot pattern appears as a combination of longitudinal and transverse structures. Note that here different mechanisms of pattern formation act in the x and in the y directions, leading to a new type of spot formation. This is different from the classical spots associated with the Turing instability only [24].

IV. LINEAR ANALYSIS

In this section we use a linear analysis to investigate conditions for the appearance of stationary solutions. Neglecting temporal dependence, we consider a solution to Eqs. (1) representing a small deviation from the basic state: $u(x,y,t)=u_S+U(y)e^{qx}$, $v(x,y,t)=v_S+V(y)e^{qx}$, where q is, in general, complex. Then $U(y)$ and $V(y)$ satisfy the equations

$$U'' = [q\Phi(y) - q^2 - j_{11}]U - j_{12}V, \qquad (9a)$$

(a)

(b)
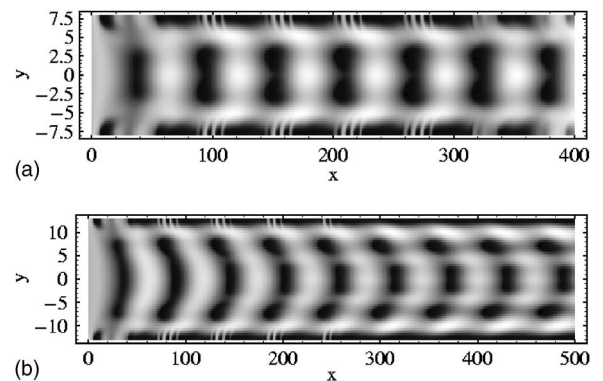
FIG. 6. The stationary spot solution as a composition of the transverse and longitudinal structures. $a=30$, $b=12$, $\delta=7$, $\phi=30$, $U_{bnd}(y) \equiv 2$, $V_{bnd}(y) \equiv 0$. (a) $h=8$, (b) $h=13$.

(a)

(b)
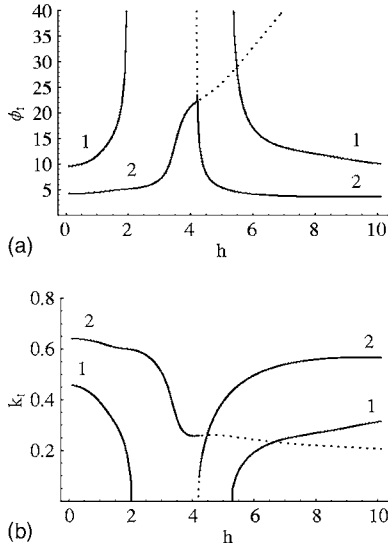
FIG. 7. (a) The critical flow rate of the transverse mode and (b) the wave number. $a=30$, $\delta=3$, (1) $b=12$, and (2) $b=7$. The transverse solution always decays in the gap between the curves 1. The dashed parts of the curves 2 indicate solutions that are not, in general, selected by the system.

$$\delta V'' = -j_{21}U + [q\Phi(y) - \delta q^2 - j_{22}]V, \qquad (9b)$$

where primes denote derivatives in y and j_{nm} are the coefficients of the Jacobian matrix, $j_{11}=3-200/(25+a^2)$, $j_{12}=-20a/(25+a^2)$, $j_{21}=2a^2b/(25+a^2)$, and $j_{22}=-5ab/(25+a^2)$. In addition, the boundary conditions,

$$U'(y=\pm h) = V'(y=\pm h) = 0, \qquad (10)$$

should be satisfied.

Transverse modes are periodic in x, so that, in general, Im $q=k\neq 0$ and Re $q=0$. Substituting $q=ik$ into Eqs. (9), we obtain a two-point boundary-value problem that has a nontrivial solution at specific values of $\phi=\phi_t$ and $k=k_t$. The eigenvalues $\phi_t>0$ and $k_t\neq 0$ are the critical flow rate and wave number, respectively, of the transverse solution. We search for the eigenvalues ϕ_t and k_t numerically by a shooting method [25] which reduces the problem to locating the zeros of a 4×4 determinant.

Figure 7 presents a numerical solution to the two-point boundary-value problem (9) and (10). Figure 7(a) shows the critical flow rate ϕ_t as a function of h and Fig. 7(b) shows the corresponding wave numbers k_t. Labels 1 and 2 indicate different values of b. It can be shown from (9) and (10) that

$$\phi_t \to 3\phi_{FDS}/2 \quad \text{and} \quad k_t \to k_{FDS}, \qquad (11)$$

as $h\to 0$, equivalent to the fact that for small h the average flow rate $(2h)^{-1}\int_{-h}^{h}\Phi(y)dy$ must exceed ϕ_{FDS}. From Eqs. (6) and (7), this gives $\phi_t\to 9.566$ and $k_t\to 0.458$ as $h\to 0$ for case 1, and $\phi_t\to 4.187$, $k_t\to 0.642$ as $h\to 0$ for case 2. An extrapolation of the numerical values obtained in Fig. 7 produced agreement with these results to within a relative precision of 10^{-5}.
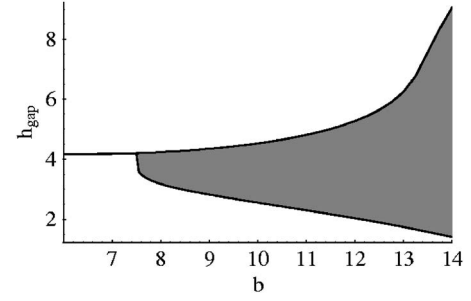
FIG. 8. The shaded area indicates a location of the gap where a nondecaying transverse solution does not exist. $a=30$, $\delta=3$.

Figure 7 shows that the transverse solution contains at least two branches. In case 1, corresponding to a higher value of b, the branches are separated with a gap where nondecaying transverse structures do not exist. The critical flow rate diverges at the edges of the gap while the wave number vanishes. When b becomes smaller, as in case 2, the branches overlap and the gap degenerates to a single point of intersection. Dashed segments of the curves correspond to transverse structures that are not, in general, selected by the system.

The numerical results of Fig. 2 correspond to either side of the gap in case 1. Figure 2(a) corresponds to the structure below the gap that is similar to a 1D FDS pattern with slight curvature in y, and Fig. 2(b) illustrates the structure that appears above the gap, where there are nonuniform transverse stripes. It is possible that the parameters used in the Poiseuille flow experiment by Kærn and Menzinger [5] correspond to the gap in solutions, and so stationary transverse structures were not observed.

The gap can be found from the conditions at its edges $\phi_t\to\infty$, $k_t\to 0$. Substituting $k_t=0$ and $\psi=\phi_t k_t$ into Eqs. (9) and keeping Re $q=0$, we obtain a new boundary-value problem for the gap edges h_{gap}. Figure 8 presents h_{gap} as a function of b. When b is decreased, the lower boundary approaches the upper one and they merge. Below this point the nonuniform transverse stripes appear before the point at which ϕ_t diverges and, as a result, the gap degenerates into a point.

Figure 7 shows only two branches of the transverse solution. The accurate numerical solution of the system (9) and (10) requires significant computational resources, especially as h increases. It is possible that a further investigation at higher values of h may reveal more branches with gaps or intersection points, but this is beyond the scope of the present study.

Let us now consider longitudinal modes. These are uniform in x and hence $q=0$. Contrary to the previous case, the transition to the longitudinal solution is not controlled by the flow rate, and the eigenvalue problem (9) and (10) determines h as a function δ, a, and b. It has a nontrivial solution $h=nh_l$ ($n=1,2,3,\ldots$), where $h_{l\pm}=\pi/(2k_{l\pm})$ and

$$k_{l\pm}^2 = [\pm\sqrt{(3a^2\delta + 5ab - 125\delta)^2 - 160a^3b\delta} + 3a^2\delta - 5ab$$
$$- 125\delta]/[2\delta(25+a^2)]. \qquad (12)$$

The requirement for h_l to be real means that k_l^2 should be real and positive. Thus, there is a critical point when the

square root vanishes, provided the rest of the expression is positive. Another critical point appears if k_{l-} or k_{l+} vanishes. However, it can be shown that this happens when the determinant of the Jacobian matrix of the system is zero, which is not relevant for a reaction-diffusion system. Here, the critical point for CIMA obtained from (12) is $\delta = \delta_l$, where

$$\delta_l = \frac{5ab[125 + 13a^2 + 4a\sqrt{10(25 + a^2)}]}{(125 - 3a^2)^2}. \qquad (13)$$

A longitudinal solution appears when $\delta > \delta_l$, i.e., this type of solution requires the differential diffusion to be sufficiently high. It can be shown that the identical critical value of δ is given by the equation $b = b_T$, where b_T is the Turing critical point (5). Hence, we conclude that the longitudinal solution is the Turing structure that fits within the channel walls.

Each k_l in (12) produces a series of longitudinal modes with profiles,

$$U(y), V(y) \propto \begin{cases} \sin[yn\pi/(2h)], & \text{for odd } n, \\ \cos[yn\pi/(2h)], & \text{for even } n, \end{cases} \qquad (14)$$

where n is the index of the longitudinal mode introduced in Sec. III. The eigenfunctions (14) can be used as inlet profiles to produce the longitudinal solutions with either an odd or even index. This works well in the numerical simulations, although this would be difficult to arrange experimentally.

In the nonlinear system higher harmonics can allow satisfaction of the boundary conditions (10) even if h does not exactly match the spectrum nh_l. Thus, nh_l gives the lower bound of h for which the longitudinal solution with corresponding index n is admitted. In particular, the smallest eigenvalue $h_l = \pi/(2k_{l+})$ determines the minimum size of the reactor for which longitudinal solutions are allowed at all.

V. SUMMARY

In this brief paper we have presented a preliminary investigation of FDS patterns in a 2D reaction-diffusion-advection system with a parabolic flow profile. Pattern formation in this system is shown to take place via two mechanisms. The first is a y-dependent version of the 1D FDS mechanism that breaks the symmetry in x along the flow. The diffusion and flow generate a spatial oscillation whose initial phase is frozen by a constant inlet condition. This results in transverse stripes similar to 1D FDS patterns. The second mechanism breaks the symmetry in y and the Turing instability produces a solution homogeneous in x that fits within the sidewalls of the channel.

The longitudinal pattern separates the reactor into areas where the concentrations of the species remain constant along the flow. It is important to note that this takes place even if the inlet distributions of the concentrations are uniform. This symmetry-breaking effect resulting in the dynamical separation of the species may be useful for experimental studies as well as in industrial processes.

When both mechanisms of pattern formation are engaged, a combination of transverse and longitudinal structures results in some interesting and complex patterns. In particular, remarkable spot patterns are observed. The 1D FDS mechanism is already known to be relevant in biological systems as a model for axial segmentation [18,19], and it is likely that the present results can also be interpreted in this context.

We believe that our results can be reproduced for other model systems and observed in experiments, although further work is first needed to examine the stability of the solutions found here. A more detailed analysis will be presented in subsequent papers.

[1] S. P. Kuznetsov, E. Mosekilde, G. Dewel, and P. Borckmans, J. Chem. Phys. **106**, 7609 (1997).

[2] P. Andresén, M. Bache, E. Mosekilde, G. Dewel, and P. Borckmanns, Phys. Rev. E **60**, 297 (1999).

[3] A. M. Turing, Philos. Trans. R. Soc. London, Ser. B **237**, 37 (1952).

[4] A. B. Rovinsky and M. Menzinger, Phys. Rev. Lett. **70**, 778 (1993).

[5] M. Kærn and M. Menzinger, Phys. Rev. E **60**, R3471 (1999).

[6] R. A. Satnoianu and M. Menzinger, Phys. Rev. E **62**, 113 (2000).

[7] R. A. Satnoianu, P. K. Maini, and M. Menzinger, Physica D **160**, 79 (2001).

[8] P. N. McGraw and M. Menzinger, to be published (2005).

[9] D. G. Míguez, R. A. Satnoianu, and A. P. Muñuzuri, submitted to Phys. Rev. Lett..

[10] P. V. Kuptsov, S. P. Kuznetsov, and E. Mosekilde, Physica D **163**, 80 (2002).

[11] P. V. Kuptsov, Physica D **197**, 174 (2004).

[12] P. V. Kuptsov and R. A. Satnoianu, Phys. Rev. E **71**, 015204(R) (2005).

[13] P. N. McGraw and M. Menzinger, submitted to Phys. Rev. E.

[14] M. Kærn and M. Menzinger, J. Phys. Chem. A **106**, 4897 (2002).

[15] J. R. Bamforth, R. Toth, V. Gaspar, and S. K. Scott, Phys. Chem. Chem. Phys. **4**, 1299 (2002).

[16] A. F. Taylor, J. R. Bamforth, and P. Bardsley, Phys. Chem. Chem. Phys. **4**, 5640 (2002).

[17] D. G. Míguez, A. P. Muñuzuri, and G. G. Izús, to be published (2005).

[18] M. Kærn, M. Menzinger, and A. Hunding, J. Theor. Biol. **207**, 473 (2000).

[19] M. Kærn, M. Menzinger, R. A. Satnoianu, and A. Hunding, Faraday Discuss. **120**, 295 (2002).

[20] L. D. Landau and E. M. Lifshitz, *Fluid Mechanics* (Pergamon-Oxford, New York, 1959).

[21] I. Lengyel and I. Epstein, Science **251**, 650 (1991).

[22] O. Jensen, V. O. Pannbacker, E. Mosekilde, G. Dewel, and P.

Borckmans, Phys. Rev. E **50**, 736 (1994).

[23] D. W. Peaceman and H. H. Rachford, Jr., J. Soc. Ind. Appl. Math. **3**, 28 (1955).

[24] J. D. Murray, *Mathematical Biology* (Springer-Verlag, New York, 1993).

[25] W. H. Press, S. A. Teukolsky, W. T. Vettering, and B. P. Flannery, *Numerical Recipes in C* (Cambridge University Press, Cambridge, 1992).